Published in final edited form as:
Health Phys. 2012 March ; 102(3): . doi:10.1097/HP.0b013e318235163f.

Hybrid Computational Phantoms Representing the Reference Adult Male and Adult Female: Construction and Applications for Retrospective Dosimetry

Jorge L. Hurtado, MS,
Department of Nuclear & Radiological Engineering, University of Florida, Gainesville, FL 32611

Choonsik Lee, PhD,
Department of Nuclear & Radiological Engineering, University of Florida, Gainesville, FL 32611

Daniel Lodwick, MS,
Department of Nuclear & Radiological Engineering, University of Florida, Gainesville, FL 32611

Timothy Goede, BS,
Department of Nuclear & Radiological Engineering, University of Florida, Gainesville, FL 32611

Jonathan L. Williams, MD, and
Department of Radiology, University of Florida, Gainesville, FL 32611

Wesley E. Bolch, PhD
Departments of Nuclear & Radiological and Biomedical Engineering, University of Florida, Gainesville, FL 32611

Abstract

Currently, two classes of the computational phantoms have been developed for dosimetry calculation: (1) stylized (or mathematical) and (2) voxel (or tomographic) phantoms describing human anatomy through mathematical surface equations and 3D voxel matrices, respectively. Mathematical surface equations in stylized phantoms are flexible but the resulting anatomy is not as realistic. Voxel phantoms display far better anatomical realism, but they are limited in terms of their ability to alter organ shape, position, and depth, as well as body posture. A new class of computational phantoms - called hybrid phantoms - takes advantage of the best features of stylized and voxel phantoms - flexibility and anatomical realism, respectively. In the current study, hybrid computational phantoms representing the adult male and female reference anatomy and anthropometry are presented. These phantoms serve as the starting framework for creating patient or worker sculpted whole-body phantoms for retrospective dose reconstruction. Contours of major organs and tissues were converted or segmented from computed tomography images of a 36-year Korean volunteer and a 25-year U.S. female patient, respectively, with supplemental high-resolution CT images for the cranium. Polygon mesh models for the major organs and tissues were reconstructed and imported into *Rhinoceros*™ for non-uniform rational B-spline (NURBS) surface modeling. The resulting NURBS/polygon mesh models representing body contour and internal anatomy were matched to anthropometric data and reference organ mass data provided by Centers for Disease Control and Prevention (CDC) and International Commission on Radiation Protection (ICRP), respectively. Finally, two hybrid adult male and female phantoms were completed where a total of 8 anthropometric data categories were matched to standard values within 4% and organ volumes matched to ICRP data within 1% with the exception of total skin. The hybrid phantoms

For reprints and correspondence contact: Wesley E. Bolch, PhD, PE, CHP Director, Advanced Laboratory for Radiation Dosimetry Studies (ALRADS) Department of Nuclear and Radiological Engineering University of Florida, Gainesville, Florida 32611-8300 Phone: (352) 846-1361 Fax: (352) 392-3380 wbolch@ufl.edu.

were voxelized from the NURBS phantoms at resolutions of 0.158 × 0.158 × 0.158 cm^3 and 0.126 × 0.126 × 0.126 cm^3 for the male and female, respectively. To highlight the flexibility of the hybrid phantoms, graphical displays are given of (1) underweight and overweight adult male phantoms, (2) a sitting position for the adult female phantom, and (3) extraction and higher-resolution voxelization of the small intestine for localized dosimetry of mucosal and stem cell layers. These phantoms are used to model radioactively contaminated individuals and to then assess time-dependent detector count rate thresholds corresponding to 50, 250, and 500 mSv effective dose, as might be needed during in-field radiological triage by first responders or first receivers.

Keywords

Hybrid phantoms; internal dosimetry; dose assessment; retrospective dosimetry

INTRODUCTION

Computational phantoms of human anatomy have been used extensively to assess the absorbed dose to individual organs received in patients undergoing imaging examinations and interventional medical procedures. The first generation of these phantoms were stylized (or mathematical) anatomic models with 3D surface equations used to describe internal organ structure and external body regions (Cristy and Eckerman 1987; Kramer *et al.* 1982; Stabin *et al.* 1995). While these equation-based phantoms provide the flexibility needed for organ repositioning and posture modification (Olsher and Van Riper 2005), they cannot provide for extremely realistic descriptions of the finer complexities of organ shape and position. The second generation of computational phantoms were voxel (or tomographic) models as introduced by several authors [see reviews by Caon (2004) and Zaidi and Xu (2007)]. Voxel phantoms are developed from cross-sectional medical images such as magnetic resonance (MR) and computed tomography (CT) scans obtained prospectively from healthy volunteers, or retrospectively from either medical patients or cadavers. Realistic anatomy of the scanned subject is faithfully implemented in the resulting voxel phantoms through the time-consuming and generally manual image-segmentation process, with subsequent coupling to Monte Carlo radiation transport codes. While they surpass stylized phantoms in anatomic realism, voxel phantoms are less flexible in terms of permitting changes in either body posture and contour, or internal organ shape, position, and depth.

A hybrid approach to phantom construction incorporates the best features of both stylized and voxel phantoms. Hybrid phantoms make use of non-uniform rational B-spline (NURBS) surfaces (Piegl 1991) to describe the boundaries of both internal organs and exterior body surfaces. NURBS is a mathematical modeling technique commonly used for generating curves and surfaces in computer animation. This technique offers mathematical approaches for representing not only standard analytic shapes, but free-form curves and surfaces, many of which are very appropriate for describing complex tissue structures. Moreover, NURBS provides the flexibility to design a large variety of shapes by manipulating individual or groups of surface control points. This feature makes it possible to more easily modify organ volumes and body contours than is possible with either stylized or voxel phantoms. For some organs such as the spine, a polygon mesh model is used in lieu of NURBS surfaces to retain the finer complexities of its 3D structure (e.g., vertebral processes and bodies). Both NURBS and polygon mesh models can collectively be used in the formation of what has been described as a *hybrid* computational phantom. Recently, our research group at the University of Florida (UF) introduced a pair of hybrid phantoms representative of a reference male and female newborn and 15-year adolescent patients (Lee *et al.* 2007; Lee *et*

al. 2008) as defined in Publication 89 of the International Commission on Radiation Protection (ICRP) (ICRP 2002). Other examples of hybrid phantoms include that of the National Library of Medicine's *Visible Human Project* by Segars (2001) and the Rensselaer Polytechnic Institute (RPI) series of pregnant female phantoms (Xu *et al.* 2007).

The objective of the present study was (1) to develop a pair of computational phantoms representing the reference adult male and female as defined in ICRP Publication 89 (ICRP 2002), and (2) use these phantoms to simulate individuals with inhaled or ingested radioactivity following the detonation of a radiological dispersion device. While several voxel phantoms have been constructed representing the ICRP reference adults (Ferrari and Gualdrini 2005; Kramer *et al.* 2004; Kramer *et al.* 2003; Schlattl *et al.* 2007), we were motivated to utilize hybrid phantom technology so that various non-reference (underweight or overweight) individuals could later be modeled rapidly and efficiently. As will be described in Bolch et al. (this issue), these hybrid phantoms were used to assess the photon energy fluence at both their anterior and posterior surfaces for five different radionuclides of interest, and all relevant source tissues. These photon fluence maps were then used to determine detector count rate efficiencies in one GM-based and three NaI-based survey meters. The ultimate goal of the study was to provide to first responders or first receivers time-dependent detector net count rates corresponding to 50, 250, and 500 mSv of effective dose for in-field radiological triage of contaminated victims.

MATERIALS AND METHODS

Anatomic Sources for Phantom Construction

In this study, the torso of the UF hybrid adult male phantom was created from segmented CT images taken from a 36-year Korean male. The chest-abdomen-pelvis (CAP) CT images were acquired on a Siemens Somatom Emotion Duo system PET/CT scanner. Korean federal regulations allow for volunteer PET/CT scanning following written informed consent. This particular volunteer was recruited for Korean reference phantom development in conjunction with a requested cancer-screening protocol. The individual was informed of all benefits and possible radiation risks associated with the imaging procedure. Subsequent images were reviewed by staff radiologists who indicated that the subject was cancer-free with the images revealing no internal abnormalities. The entire image set consisted of 250 CT image slice, each 3-mm in slice thickness and of a matrix size of 512 × 512 pixels. Major organs and tissues were segmented within the CT data set using *3D-DOCTOR*™ (Able Software, Lexington, MA), a 3D modeling and imaging software package. Contour files generated in *3D-DOCTOR*™ were then converted to polygon mesh models as *Wavefront Object* files and imported to *Rhinoceros*™ (McNeel North American, Seattle, WA), a NURBS modeling, rendering, and analysis software package. As an alternative to the head CT images of the Korean volunteer, higher-resolution CT images (1-mm slice thickness) were taken from an 18-year cadaver image set to develop the head model of the UF hybrid adult male phantom.

The torso of the UF hybrid adult female phantom was segmented from head and CAP CT images of a 25-year female subject. Candidate CT data sets were selected from images archived in the University of Florida's Department of Radiology, and were reviewed under IRB-approved and HIPAA-compliant protocols. Selected image sets, based on gender and age, were reviewed by an experienced radiologist for abnormal patient anatomy. Scans with organs which may have been affected by local or systemic diseases were discarded, as well as those indicating trauma or other abnormalities. The selected CT images were further reviewed to select patients that displayed sitting heights relatively close to mean values for the U.S. adult female population as tabulated by the Centers for Disease Control and Prevention (http://www.cdc.gov/nchs/nhanes.htm). The CT data used for construction of the

female phantom consisted of 258 4.5-mm CT image with an in-plane matrix size of 512 × 512 pixels. Organ segmentation and conversion of contour file to polygon mesh and NURBS models were similar to those used in the building of the adult male phantom. In addition, high-resolution head CT images from a 14-year female patient were adopted to develop the head model of the hybrid adult female phantom. The resulting head model was scaled upward to match reference anthropometric and other anatomical data for the adult female.

Both the 36-year male and 25-year female patients, whose anatomy was incorporated into the reference hybrid phantoms, were scanned in a supine position with arms raised for the CAP exams and at the patient's side for the head exams. Moreover, the CT scans did not extend to the lower limbs. As a result, the arms and legs were not available in the selected CT data sets for phantom construction, and thus extremities for both phantoms were imported from high-resolution CT scans of an 18-year male cadaver. The arms (820 slices) and legs (1099 slices) were reconstructed each at 1.0-mm slice thickness. The arm and leg bones in the CT images were carefully segmented and the resulting polygon mesh models were attached to the torso of the adult male and female phantoms at the NURBS modeling stage.

Further anatomical detail of the spinal column (both vertebrae and intravertebral discs) was sought following a review of the original segmented spines in both phantoms. Consequently, the entire spinal column in the male phantom was replaced by that segmented from an 18-year male cadaver at 1-mm slice thickness. For the female phantom, spinal data from a 14-year female (cervical series) and a 13.7-year female (thoracic and lumbar series) were segmented, volumetrically rescaled, and inserted into the adult female hybrid phantom. The resulting steps yielded superior anatomic detailed in the final phantom design.

NURBS Surface Modeling

The UF adult hybrid phantoms were constructed using similar modeling methods and an identical organ list to that defining the UF newborn and 15-year hybrid phantoms (Lee *et al.* 2007; Lee *et al.* 2008), with separate gender-specific image sources employed for each phantom. All organs and tissues imported from *3D-Doctor*™ in polygon mesh format were converted to NURBS surfaces with the exclusion of the skeleton, brain, and extrathoracic airways as the details and shapes of their original anatomy could not be modeled efficiently via NURBS surfaces. For all remaining tissues, organ contours were obtained from the imported polygon mesh objects and then NURBS surfaces were generated from those contours, thus maintaining their original anatomic realism.

As for paired organs other than the lungs, right and left organs were forced to be of equivalent volumes and positions in the UF hybrid adult phantoms. These included selected bone sites (clavicles, scapulae, arm and leg bones, and ribs), salivary glands, testes (male), scrotum (male), ovaries (female), eye balls, eye lens, and tonsil. The positions and volumes of the right organs were matched to those of the left organs except for the kidneys and adrenals for which the left organs are generally superior in position to those on the patient's right. Organs and tissues whose anatomical shapes are theoretically close to stylistic and simple 3D surfaces were represented by simple NURBS objects such as spheres and ellipsoids. This stylistic approach was attempted for the sex-specific organs (breast, penis, scrotum, testes, and ovaries) and the other selected tissues (urinary bladder, eye balls, lens, tongue, tonsil, and pituitary gland). Special modeling approaches were attempted for the respiratory and alimentary organ systems for which the original segmentation was anatomically poor in representing their original shapes and positions. A detailed description of our NURBS modeling approaches for these organ systems is documented in our study of the reference newborn (Lee *et al.* 2007).

The skeleton was modeled as a homogeneous mixture of cortical bone, trabecular bone, active and inactive bone marrow, teeth, and miscellaneous skeletal tissues. All bone sites were modeled via polygon mesh surfaces, with the exception of the ribs, which were modeled using NURBS surfaces. The latter approach was chosen as the inter-rib spacing was generally less than the original CT image slice thickness. Central contours and cross-sections of ribs were carefully obtained from the original polygon-mesh model, and pipe-shaped NURBS surfaces of the desired cross-sectional area were generated. NURBS surfaces for the ribs were running from the vertebral body of the thoracic spine to the beginning of the costal cartilage at near the sternum. After the costal cartilage regions and ribs were separated, the total mass of the NURBS rib-cage model was calculated and matched to that of the original ribs through adjustments in the cross-sectional area of each rib. One additional site of skeletal cartilage was explicitly modeled in each phantom – that of the inter-vertebral discs of the spine, as segmented from the original CT data. Unlike the UF newborn hybrid phantom, bone-associated cartilage (which for the adult would be predominately found at joints, tendons, and ligaments) was not modeled explicitly, but was considered in the tissue category *residual soft tissues* as described below.

Standardization of Hybrid Phantoms

Once all organs and tissues were modeled by NURBS or polygon mesh surfaces, the male and female phantoms were matched to anthropometric data obtained from several literature sources and reference organ masses given in ICRP Publication 89 (ICRP 2002). First, a body contour that permitted independent changes to the head, torso, and limb dimensions to match either reference and/or patient-specific values was developed. Currently a total of eight anthropometric data are available for the adult male and female: heights (standing and sitting), lengths (total arm), circumferences (head, neck, waist, buttock), and biacromial breadth. Of these, ICRP Publication 89 provides only standing height. Sitting height and waist circumference were provided by the National Health and Nutrition Examination Survey (NHANES) IV series while the buttock circumference and biacromial breadth was provided by the NHANES III data series (http://www.cdc.gov/nchs/nhanes.htm). Head circumference data for the adult phantoms were taken from study by Eichorn and Bayley (1962). The arm lengths, which included individual measurements of acromion-radiale, radiale-stylion, and hand lengths, were provided by the U.S. Army's anthropometric data survey (Gordon *et al.* 1989). Neck circumference data were taken for 20-year-olds as reported in the anthropometric database Anthrokids by the U.S. Consumer Product Safety Commission (http://www.itl.nist.gov/div894/ovrt/projects/anthrokids). All of the anthropometric parameters in the UF hybrid adult male and female phantoms were matched to 50^{th} percentile values within a relative error of no more than 3% as shown in Table 1.

Once body dimensions of both adult phantoms were matched to standard anthropometric data, the volumes of individual organs and tissues were adjusted to match those given in ICRP Publication 89 (ICRP 2002) within a tolerance of 1%. Reference densities provided in ICRU Report 46 (ICRU 1992) were used to calculate target organ volumes given their corresponding reference masses. An effective density of 0.38 g cm^{-3} was assigned to the lungs in both phantoms so as to force a match to reference lung masses (inclusive of blood content). We note that this is the same effective density used in the Rex and Regina reference voxel phantoms (Schlattl *et al.* 2007). An effective density was also assigned to the content of the small intestine, right and left colon, and recto-sigmoid colon. In contrast, the mass of the stomach contents was matched to its reference value by adjustment of the level of content from the base of the stomach with the residual space assigned to air. Lengths of the esophagus, small intestine, right colon, left colon, and recto-sigmoid colon were matched to their ICRP 89 reference lengths to within ±4%. These reference lengths are 28 and 26 cm for the male and female esophagus, 280 and 260 cm for the male and female

small intestine, 34 and 30 cm for the male and female right colon, 28 and 25 cm for the male and female left colon, and 38 and 35 cm for the male and female recto-sigmoid colon, respectively. Each of the parotid, submaxillary, and sublingual glands comprising the salivary glands was matched to their individual reference values in ICRP Publication 89. Regions not explicitly segmented in the phantom were termed *residual soft tissue* (RST) and include separable fat, skeletal muscle, connective tissue, fixed lymphatic tissues, large blood vessels, and bone-associated cartilage. The latter excludes cartilage of the ears, external nose, larynx, pharynx, trachea, coastal cartilage of the ribs, and inter-vertebral discs, all of which are explicitly modeled in the hybrid phantoms. The elemental composition and mass density of the RST was determined as volume-weighted averages of these tissue constituents.

The reference skin thicknesses for the adult male and female phantoms were derived from three other reference parameters, namely the ICRP 89 skin mass (3300 g for the male and 2300 g for the female), body surface area (1.90 m^2 for the male and 1.66 m^2 for the female) and the skin density (1.1 g cm^{-3} for both the male and female). The resulting reference skin thicknesses were 0.158 cm and 0.126 cm for adult male and female phantoms, respectively. The skin volumes of the UF hybrid phantoms were able to be obtained only in their voxelized format created from the corresponding NURBS phantom via a *voxelization* process described previously by Lee et al. (2007) The phantom's skin layer (dermis and epidermis) was generated by assigning a skin tag to the outermost voxel layer during the voxelization process. As the skin was the thinnest tissue layer to be represented in the final hybrid voxel phantoms, the voxel resolutions of the entire phantoms were set at 0.158 cm and 0.126 cm for adult male and female, respectively.

The resulting total body masses were thus 73.007 kg and 60.017 kg for male and female, respectively, which are 0.009% and 0.029% higher than the corresponding ICRP 89 reference values (73 kg for male and 60 kg for female), respectively. It is further noted that these ICRP 89 reference total body masses are slightly higher than 50th percentile values in the 20-year U.S. males and 20-year U.S. females, which are 71 kg and 58 kg, respectively (www.cdc.gov/growthcharts). ICRP reference total heights – 176 cm for the adult male and 163 cm for adult female – are equivalent to their 50th percentile values for 20-year U.S. male and female adults.

Voxelization of Hybrid Phantoms

The voxelization process is crucial for the resulting NURBS phantoms to be ported to radiation transport codes as currently there are no Monte Carlo codes available that can directly handle NURBS or polygon mesh geometry for radiation transport. A procedure presented previously for the UF hybrid newborn phantom was adopted in this study (Lee *et al.* 2007) using an upgraded in-house MATLAB code, *Voxelizer 4*, where speed-up algorithms and additional user-friendly features were implemented. All objects in the phantom were saved in one ASCII *Raw Triangles* file and voxelized simultaneously. The meshing tolerance (MT) was set at 10 degrees based on our previous sensitivity study in order to minimize the possibility of volumetric errors exceeding 1% across all organs of the voxelized phantoms. As mentioned above, voxel resolutions were set at 0.158 cm and 0.126 cm for adult male and female phantoms, respectively, as based on their respective reference skin thicknesses. After voxelization, the skin tag was assigned to the single outermost voxel layer of each phantom. Approximately two to three hours of voxelization time was required for both phantoms using a computer cluster system which includes a head node / eight slave node setup equipped with Red Hat Linux, PGI compilers, two 2.2Ghz AMD dual cores with 2GB RAM per core.

In the present study, we have adopted the following acronyms for the University of Florida Hybrid Computational Phantoms of the reference Adult Male and Female – UFHADM and UFHADF, respectively. As will be discussed below, alterations of the phantoms' outer body contours and reassignment of residual soft tissue densities permit one to model other body profiles and tissue compositions (skeletal muscle and adipose tissue) that are unique to individual subjects or to other weight percentile means in the U.S. population.

RESULTS

Frontal views of the UFHADM and UFHADF phantoms are shown in Fig. 1 with semi-transparent skin and residual tissue for improved viewing of internal organ structure. Cross-sectional representations of both phantoms are given in Figs. 2 to 4 showing a single transaxial, the mid-coronal, and the mid-sagittal views, respectively, each with organ labeling.

Organ masses of the UF hybrid-NURBS and hybrid-voxel male and female phantoms are compared to those given in ICRP Publication 89 in Tables 2 and 3, respectively. Percent differences between hybrid phantoms and ICRP 89 values are evaluated in columns 5 to 8 in both tables. All body organs and tissues are shown to be matched to within ±1% with the exception of the skin (11.7% and 11.8% larger for the male and female, respectively). Brain masses – which were smaller than ICRP 89 reference values in the case of the UF newborn phantoms – were matched to within 1% in these UF adult hybrid phantoms.

DISCUSSION

As noted previously, hybrid phantoms retain the anatomical realism of image-segmented voxel phantoms, while preserving flexibility traditionally available only to equation-based stylized phantoms. Three advantageous features of hybrid phantoms are graphically demonstrated below. These include (1) the ability to model underweight and overweight (i.e., non-50^{th} percentile) individuals during reconstruction of external or even internal exposures, (2) the ability to reposition the arms and legs of the phantom to represent unique worker or patient-specific exposure postures, and (3) the ability to extract individual organs or sets of organs from the whole-body phantom and voxelize those tissues at a significantly higher resolution than would be computationally permitted within a full-body phantom. Brief examples of each are give below. Again, each feature can be performed using traditional stylized phantoms and organ models, yet with hybrid phantoms, these tasks can be achieved rapidly without sacrifice of anatomical structure.

In the UF hybrid phantom series, skeletal muscle is intentionally not segmented from the original CT images, and is thus purposefully included in *residual soft tissues* (RST). Our rationale for this approach is that while skeletal muscle is one of the remainder tissues in the definition of the effective dose (ICRP 2007), this tissue is of very low radiobiological significance, and primarily serves to attenuate and scatter radiation fields entering the body. Furthermore, explicit representation of skeletal muscles in either NURBS or polygon mesh formats would exceedingly complicate volumetric rescaling of a reference 50^{th} percentile phantom in modeling either underweight or overweight individuals during dose reconstruction. Instead, the outer body contour of the hybrid phantom can be repositioned, via inward or outward movement of the NURBS surface control points, thus decreasing or increasing RST volume in the phantom, respectively. This technique is similar to that suggested for stylized phantoms (Van Riper 1999; Van Riper *et al.* 1996), but with hybrid phantoms, the adjustments can be highly unique to the individual and body-region. As an example, Fig. 5 shows two morphed versions of the UFHADM phantom – one of lower total body weight (left) and one of significantly higher total body weight (right). Additionally, the

elemental composition of RST in these non-reference phantoms can be uniquely adjusted in regard to the percent distribution of adipose tissue and skeletal muscle, thus allowing one to model the body composition of a given individual. One additional complication in modeling overweight adult subjects, however, is that increases in adipose tissue appear as both subcutaneous fat (accommodated through outer-body contour adjustments) and intra-abdominal fat (which in principle must be accommodated through re-arrangement of abdominal organs in the reference phantom). These changes in the UF reference hybrid phantoms will be indicated via numerical subscripts. For example, the phantom $UFHADM_{50\text{-}90}$ will denote a phantom matching the 50^{th} height and 90^{th} weight percentile of U.S. adult males.

A second feature of hybrid phantoms is their ability to permit repositioning of the arms and legs. Such methods exist presently for equation-based stylized anthropomorphic phantoms (Akkurt and Eckerman 2007; Olsher and Van Riper 2005). With hybrid phantoms, similar rearrangement of the extremities can be performed as demonstrated graphically in Fig. 6 for a sitting version of the UFHADF phantom. Movement of the extremities is performed in two phases. First, the arm and/or leg bones are repositioned, and then second, the control points defining the outer surface of the extremities are repositioned as well. The absence of muscle structures in the phantom's arms and legs again facilitates these alternations of phantom posture. The fingers of the phantom can even be repositioned to represent grasping (e.g., tools) or holding (e.g., medical syringe) for unique worker-specific exposure scenarios. Other applications might include modeling of chair-based whole-body counters, modeling of cosmic-ray exposures to seated aircraft or spacecraft crew members, and modeling of radiation exposures to patients with arms extended upward during medical imaging.

A third important advantage of hybrid phantoms in their NURBS / polygon mesh format is the ability to voxelize organs and tissues at any user-defined dimension. One example is shown schematically in Fig. 7 where the small intestine of the UF hybrid male phantom has been extracted from the whole-body model, and one additional NURBS surface inserted defining the small intestine mucosal layer. Such fine anatomical structures are needed for local beta-particle dosimetry in the small intestine, where typically single or packed cylindrical models of intestinal segments must be used for dose assessment (Jönsson *et al.* 2002). As shown in Fig. 7, however, the same small-intestine model used the phantom for photon and perhaps neutron dosimetry, can be employed for regional beta-particle and even alpha-particle dosimetry, but at a much higher voxel resolution than would be feasible in the whole-body phantom.

Future work will include the following updates to the reference adult phantoms presented here. First, the breasts in the adult female phantom will be updated to represent a more realistic external shape, with additional partitioning of the breast tissue into glandular and adipose components. Second, revisions to the small intestine are underway to reduce inter-segment tissue spacing. Third, a lymphatic node model will be added with removal of this organ from residual soft tissues (Bolch *et al.* 2008). Finally, work on a detailed and NURBS-based lung tree is underway given bronchial and bronchiolar segment lengths and diameters as defined in ICRP Publication 66 (ICRP 1994).

CONCLUSIONS

In this study, we present two new computational reference phantoms – those of the ICRP reference adult male and female – created in a hybrid format using combinations of polygon mesh and NURBS surface models of internal organs and exterior body region contours. Both phantoms were assembled using segmented CT images of live patients, and were matched to reference anatomic data from ICRP Publication 89 and various anthropometric

sources to within tolerances of 1% and 4%, respectively. As presented in Bolch et al. (this issue), these phantoms are used in the construction of survey meter detector efficiencies for five radionuclides and various source tissues, as well as time-dependent detector thresholds corresponding to predicted effective doses of 50, 250, and 500 mSv. Through the repositioning of NURBS control points on the exterior surfaces of these hybrid phantoms, other adult subjects of higher or lower weight percentiles can be easily modeled, and detector count rates re assessed, giving further guidance and accuracy to the interpretation of survey meter count rates during post-event and in-field radiological triage by first responders or first receivers.

Acknowledgments

This work was performed under contract TKC 30-06 16601 CDC Task 29 with TKC Integration Services, Inc. and the U.S. Centers for Disease Control and Prevention.

This work was supported by the TKC Integration Services, Inc.

References

Akkurt, H.; Eckerman, KF. Development of PIMAL: Mathematical phantom with moving arms and legs. Oak Ridge National Laboratory; Oak Ridge, TN: 2007. ORNL/TM-2007/14

Bolch WE, Hurtado JL, Lee C, Manger R, Hertel N, Dickerson W. Guidance on the use of hand-held survey meters for radiological triage: Time-dependent detector count rates correspondign to 50, 250, and 500 mSv effective dose for adult males and adult females. Health Phys. (this issue)

Bolch WE, Lee C, Pafundi DH, Padilla L. Anatomic models of the lymphatic nodes within the UF adult and pediatric hybrid phantoms – Applications to lymphoma patient dosimetry [Abstract]. Eur J Nucl Med. 2008; 35:S135.

Caon M. Voxel-based computational models of real human anatomy: a review. Radiat Environ Biophys. 2004; 42:229–235. [PubMed: 14730450]

Cristy, M.; Eckerman, KF. Specific absorbed fractions of energy at various ages from internal photon sources. Vol. Volumes I-VII. Oak Ridge National Laboratory; Oak Ridge, TN: 1987. ORNL/TM-8381/

Eichorn DH, Bayley N. Growth in head circumference from birth through young adulthood. Child Dev. 1962; 33:257–271. [PubMed: 13889573]

Ferrari P, Gualdrini G. An improved MCNP version of the NORMAN voxel phantom for dosimetry studies. Phys Med Biol. 2005; 50:4299–4316. [PubMed: 16148395]

Gordon, CG.; Churchill, T.; Clauser, CE.; Bradtmiller, B.; McConville, JT.; Tebbetts, I.; Walker, RA. 1988 Anthropometric Survey of U.S. Army Personnel. U.S. Army Natick RD&E Center; Natick, MA: 1989. NATICK/TR-89/027

ICRP. ICRP Publication 66: Human respiratory tract model for radiological protection. Ann ICRP. 1994; 24:1–482.

ICRP. ICRP Publication 89: Basic anatomical and physiological data for use in radiological protection - reference values. Ann ICRP. 2002; 32:1–277.

ICRP. ICRP Publication 103: Recommendations of the International Commission on Radiological Protection. Annals of the ICRP. 2007; 37:1–332.

ICRU. Photon, electron, proton and neutron interaction data for body tissues. International Commission on Radiation Units and Measurements; Bethesda, MD: 1992. Report 46

Jönsson L, Liu X, Jonsson BA, Ljungberg M, Strand SE. A dosimetry model for the small intestine incorporating intestinal wall activity and cross-doses. J Nucl Med. 2002; 43:1657–1664. [PubMed: 12468516]

Kramer R, Khoury HJ, Vieira JW, Loureiro EC, Lima VJ, Lima FR, Hoff G. All about FAX: a Female Adult voXel phantom for Monte Carlo calculation in radiation protection dosimetry. Phys Med Biol. 2004; 49:5203–5216. [PubMed: 15656272]

Kramer R, Vieira JW, Khoury HJ, Lima FR, Fuelle D. All about MAX: a male adult voxel phantom for Monte Carlo calculations in radiation protection dosimetry. Phys Med Biol. 2003; 48:1239–1262. [PubMed: 12812444]

Kramer, R.; Zankl, M.; Williams, G.; Drexler, G. Part I: The male (ADAM) and female (EVA) adult mathematical phantoms. Gesellschaft für Strahlenund Umweltforschung; Munich: 1982. The calculation of dose from external photon exposures using reference human phantoms and Monte Carlo methods. GSF-Bericht-S-885

Lee C, Lodwick D, Hasenauer D, Williams JL, Lee C, Bolch WE. Hybrid computational phantoms of the male and female newborn patient: NURBS-based whole-body models. Phys Med Biol. 2007; 52:3309–3333. [PubMed: 17664546]

Lee C, Lodwick D, Williams JL, Bolch WE. Hybrid computational phantoms of the 15-year male and female adolescent: applications to CT organ dosimetry for patients of variable morphometry. Med Phys. 2008; 35:2366–2382. [PubMed: 18649470]

Olsher RH, Van Riper KA. Application of a sitting MIRD phantom for effective dose calculations. Radiat Prot Dosimetry. 2005; 116:392–395. [PubMed: 16604666]

Piegl L. On NURBS: A survey. IEEE Comp Graph Appl. 1991; 11:55–71.

Schlattl H, Zankl M, Petoussi-Henss N. Organ dose conversion coefficients for voxel models of the reference male and female from idealized photon exposures. Phys Med Biol. 2007; 52:2123–2145. [PubMed: 17404459]

Segars, WP. Development and application of the new dynamic NURBS-based cardiac-torso (NCAT) phantom [Dissertation]. University of North Carolina; Chapel Hill, NC: 2001.

Stabin, M.; Watson, E.; Cristy, M.; Ryman, J.; Eckerman, K.; Davis, J.; Marshall, D.; Gehlen, M. Mathematical models and specific absorbed fractions of photon energy in the nonpregnant adult female and at the end of each trimester of pregnancy. Oak Ridge National Laboratory; Oak Ridge, TN: 1995. ORNL/TM-12907

Van Riper, KA. BodyBuilder. Version 1.0. White Rock Science; White Rock, NM: 1999. Version

Van Riper, KA.; Spikes, DL.; McDowell, RG. Advances and Applications in Radiation Protection and Shielding. American Nuclear Society; 1996. Variable human anthropomorphic models; p. 643

Xu XG, Taranenko V, Zhang J, Shi C. A boundary-representation method for designing whole-body radiation dosimetry models: pregnant females at the ends of three gestational periods--RPI-P3, -P6 and -P9. Phys Med Biol. 2007; 52:7023–7044. [PubMed: 18029991]

Zaidi H, Xu XG. Computational anthropomorphic models of the human anatomy: the path to realistic Monte Carlo modeling in radiological sciences. Annu Rev Biomed Eng. 2007; 9:471–500. [PubMed: 17298237]

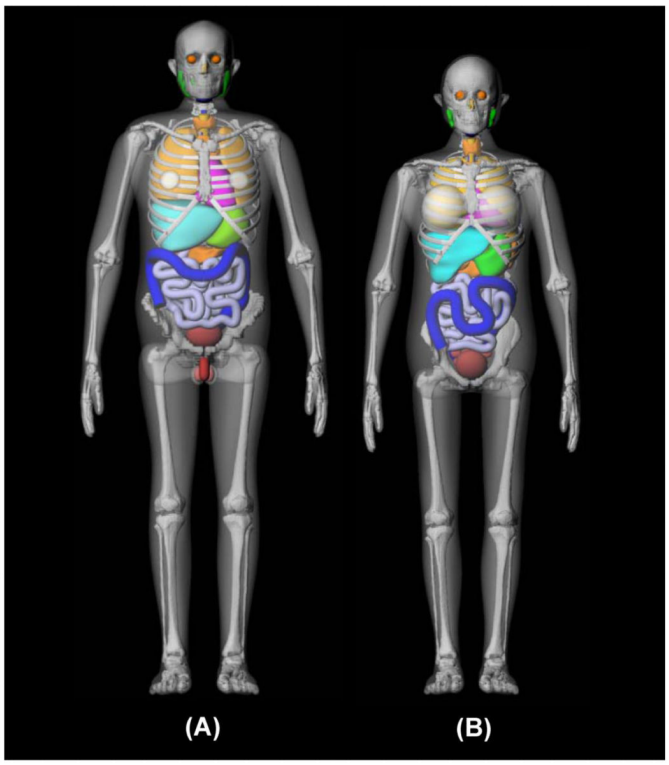

Figure 1.
Frontal views following 3D rendering of **(A)** UF hybrid adult male phantom and **(B)** UF hybrid adult female phantom. Body contours are made transparent for improved viewing internal organs and the skeleton.

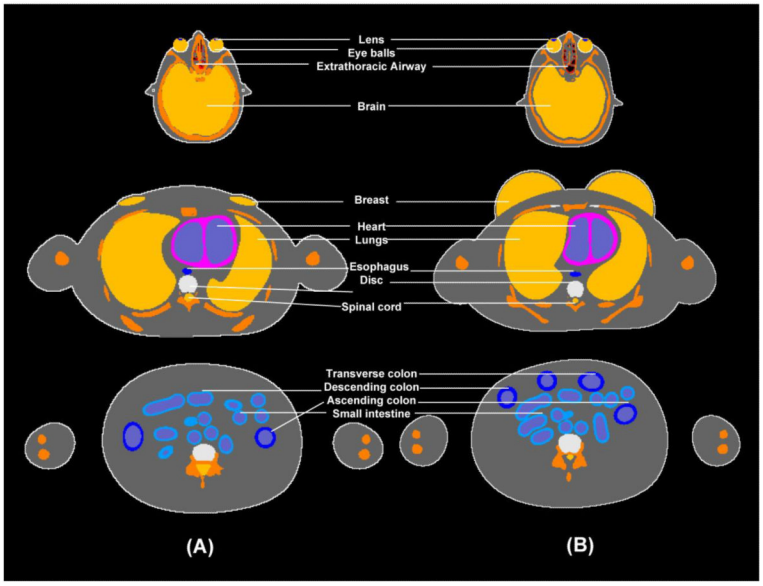

Figure 2.
Transaxial views (cross sections) of the voxelized hybrid adult **(A)** male and **(B)** female phantoms.

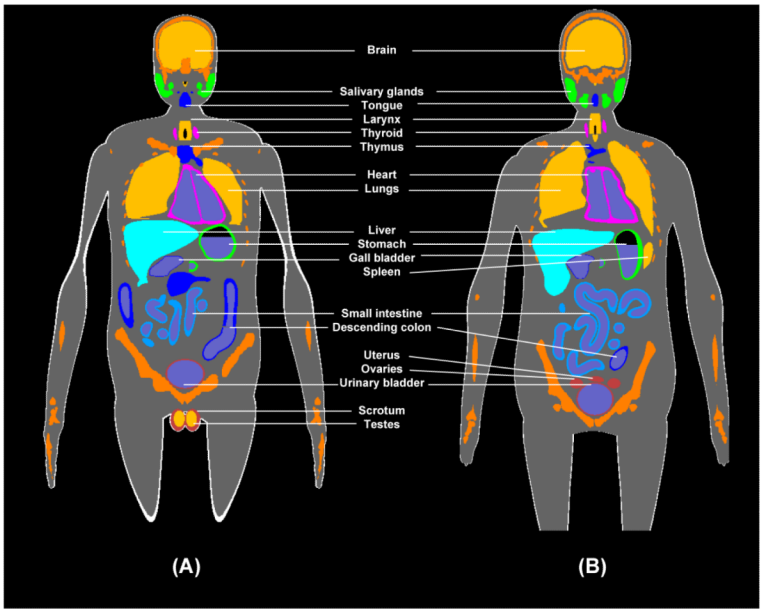

Figure 3.
Coronal views (cross sections) of the voxelized hybrid adult **(A)** male and **(B)** female phantoms.

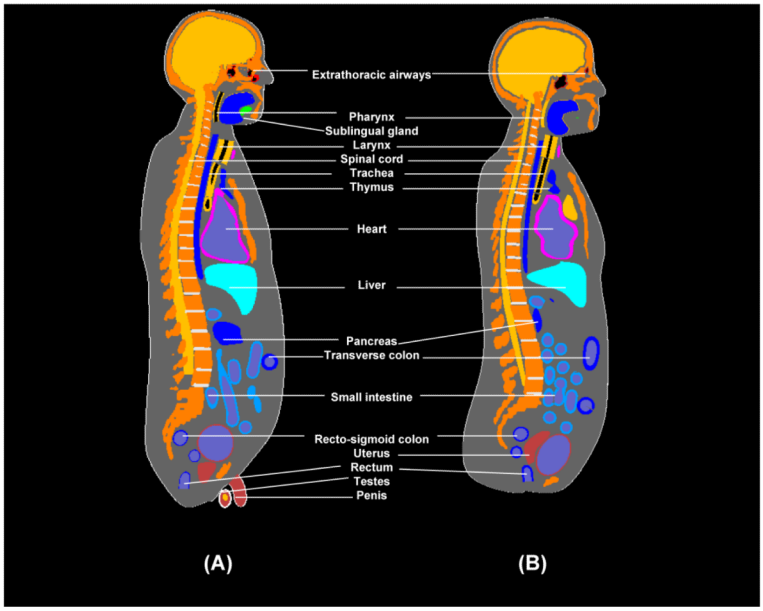

Figure 4.
Sagittal views (cross sections) of the voxelized hybrid adult **(A)** male and **(B)** female phantoms.

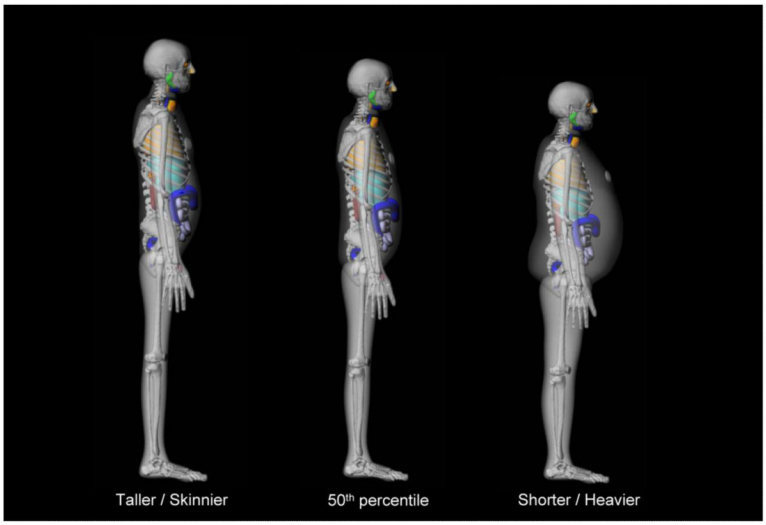

Figure 5.
Lateral views showing 3D rendering of the UF hybrid male phantom at total body masses less than and greater than the ICRP 89 reference value of 73 kg.

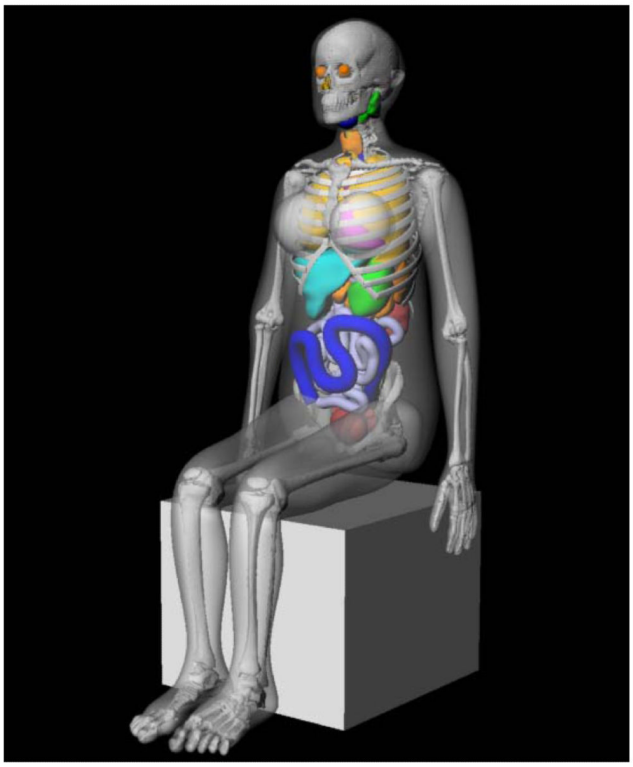

Figure 6.
View of the UF hybrid female phantom shown in a sitting position as potentially needed for individualized, posture-dependent reconstruction of external radiation exposures.

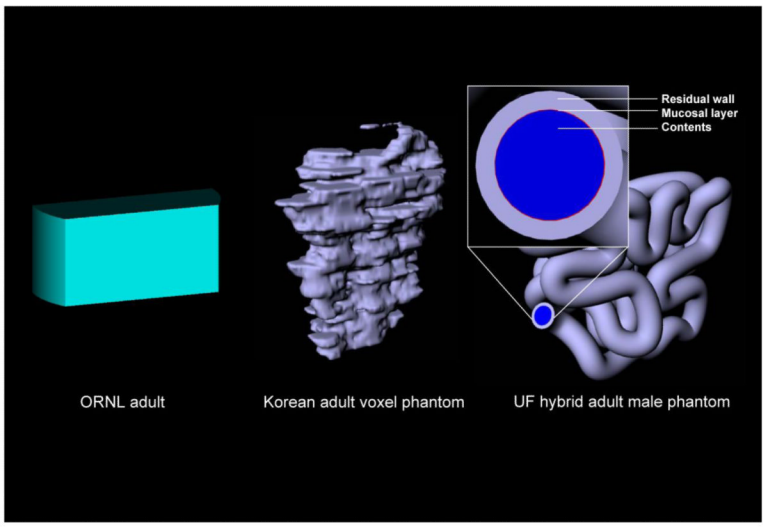

Figure 7.
Graphical comparison of the small intestine within the ORNL stylized adult phantom, a voxel phantom of a Korean adult volunteer, and the UF hybrid phantom. For the latter, it is possible to remove the small intestine from the whole-body model and voxelize the structure at much higher resolution as required to model tissues of the radiosensitive mucosal layer.

Table 1

Reference anthropometric parameters for the adult male and female as obtained from various literature sources and the values realized in the final UF hybrid phantoms.

		Reference values		UF Hybrid phantoms			
Anthropometric parameters		**Male**	**Female**	**Male**	**RE (%)**	**Female**	**RE (%)**
Height	Standing[a]	176.0	163.0	176.0	0.0	163.0	0.0
	Sitting[b]	91.9	86.1	92.0	0.1	85.5	−0.7
Length	Total arm[c]	80.1	73.5	80.9	1.0	72.9	−0.8
Circumference	Head[d]	57.2	56.1	57.4	0.3	56.2	0.3
	Neck[e]	36.6	31.4	36.8	0.5	31.9	1.4
	Waist[b]	92.5	87.1	92.1	−0.4	88.8	2.0
	Buttock[f]	96.0	97.6	96.0	0.0	95.6	−2.0
Breadth	Biacromial[f]	40.8	36.4	39.8	−2.5	35.8	−1.6

[a] ICRP89

[b] NHANES IV (1999-2002)

[c] US Army anthropometric data survey (1989)

[d] Eichorn and Bayley (1962)

[e] ANTHROKIDS (1977)

[f] NHANES III (1988-1994)

Table 2

Summary of organ masses within two computational phantoms of the adult reference male: (1) UF Hybrid-NURBS and (2) UF Hybrid-Voxel. These organ masses are then compared to those in ICRP Publication 89 by organ, organ system, and for total body tissues (exclusive of walled-organ content), and total body mass (inclusive of wall-organ content).

Organ System	Density (g/cm^3)	Comment (ICRU 46)	Target Volume (cm^3)	UFH - NURBS mass (g)	% Diff	UFH - Voxel mass (g)	% Diff	ICRP 89 mass (g)
Respiratory System								
ET1 (anterior nasal layer)	1.03	*ICRU-46 ave soft tissue*		0.43		0.54		ND
ET2 (posterior nasal layer)	1.03	*ICRU-46 ave soft tissue*		17.56		16.00		ND
ET2 (oral cavity layer)	1.03	*ICRU-46 ave soft tissue*		1.37		1.46		ND
ET2 (larynx)	1.07	*50:50 soft tissue/cartilage*	26.29	28.12	0.4%	28.17	0.6%	28.0
ET2 (pharynx)	1.03	*ICRU-46 ave soft tissue*		3.48		3.61		ND
Trachea	1.07	*50:50 soft tissue/cartilage*	9.39	9.96	−0.4%	9.97	−0.3%	10.0
Bronchi - extrapulmonary	1.07	*50:50 soft tissue/cartilage*		10.44		10.39		ND
Lungs (inclusive of blood)	0.38	*calculated*		1200.00	0.0%	1196.09	−0.3%	1200.0
Left Lung	0.38	*calculated*		502.32	−10.0%	501.76	−10.1%	558.1
Right Lung	0.38	*calculated*		697.68	8.7%	694.32	8.2%	641.9
Alimentary System								
Tongue	1.05	*muscle*	69.52	73.16	0.2%	72.47	−0.7%	73.0
Salivary glands	1.03	*ICRU-46 ave soft tissue*	82.52	84.93	−0.1%	84.50	−0.6%	85.0
Parotid	1.03	*ICRU-46 ave soft tissue*	48.54	49.97	−0.1%	49.66	−0.7%	50.0
Submaxillary	1.03	*ICRU-46 ave soft tissue*	24.27	24.98	−0.1%	24.91	−0.3%	25.0
Sublingual	1.03	*ICRU-46 ave soft tissue*	9.71	9.98	−0.2%	9.92	−0.8%	10.0
Tonsils	1.03	*ICRU-46 ave soft tissue*	2.91	3.02	0.5%	2.98	−0.8%	3.0
Esophagus - wall	1.03	*gastrointestine (adult)*	38.83	39.98	−0.1%	40.11	0.3%	40.0
Stomach - wall	1.03	*gastrointestine (adult)*	145.63	150.41	0.3%	149.93	0.0%	150.0
Stomach - contents	1.03	*ICRU-46 ave soft tissue*	242.72	250.13	0.1%	251.59	0.6%	250.0
Small Intestine - wall	1.03	*gastrointestine (adult)*	631.07	653.65	0.6%	646.96	−0.5%	650.0
Small Intestine - contents	0.48	*ICRU-46 ave soft tissue*	736.02	350.00	0.0%	348.98	−0.3%	350.0
Colon								
Right - wall	1.03	*gastrointestine (adult)*	145.63	150.31	0.2%	149.65	−0.2%	150.0
Right - contents	0.74	*ICRU-46 ave soft tissue*	201.63	150.00	0.0%	149.31	−0.5%	150.0
Left - wall	1.03	*gastrointestine (adult)*	145.63	150.17	0.1%	149.43	−0.4%	150.0
Left - contents	0.56	*ICRU-46 ave soft tissue*	134.14	75.00	0.0%	75.13	0.2%	75.0
Rectosigmoid - wall	1.03	*gastrointestine (adult)*	67.96	69.89	−0.2%	69.52	−0.7%	70.0
Rectosigmoid - contents	0.45	*ICRU-46 ave soft tissue*	167.35	75.00	0.0%	74.63	−0.5%	75.0
Liver	1.06	*liver (fetus/child/adult)*	1698.11	1802.64	0.1%	1799.68	0.0%	1800.0
Gall Bladder - wall	1.03	*ICRU-46 ave soft tissue*	9.71	10.05	0.5%	9.98	−0.2%	10.0
Gall Bladder - contents	1.03	*ICRU-46 ave soft tissue*	56.31	58.02	0.0%	58.06	0.1%	58.0
Pancreas	1.03	*ICRU-46 ave soft tissue*	135.92	140.10	0.1%	139.76	−0.2%	140.0
Circulatory System								

Organ System	Density (g/cm^3)	Comment (ICRU 46)	Target Volume (cm^3)	UFH - NURBS mass (g)	% Diff	UFH - Voxel mass (g)	% Diff	ICRP 89 mass (g)
Heart - wall	1.05	*heart (fetus/child/adult)*	314.29	330.20	0.1%	330.40	0.1%	330.0
Heart - content	1.06	*blood (newborn/adult)*	481.13	509.44	−0.1%	508.32	−0.3%	510.0
Urogenital System								
Kidneys (Cortex+Medulla)	1.05	*kidney (fetus/child/adult)*	295.24	309.81	−0.1%	309.33	−0.2%	310.0
Cortex (70%)	1.05	*kidney (fetus/child/adult)*	217.54	228.08	−0.1%	227.75	−0.3%	228.4
Medulla (25%)	1.05	*kidney (fetus/child/adult)*	77.69	81.73	0.2%	81.58	0.0%	81.6
Pelvis (5%)	1.05	*kidney (fetus/child/adult)*	15.54	16.31	0.0%	16.28	−0.2%	16.3
Urinary Bladder - wall	1.04	*bladder (adult-empty)*	48.08	50.12	0.2%	49.69	−0.6%	50.0
Urinary Bladder - contents[a]	1.01	*urine of ave density*	200.99	202.64	−0.2%	201.77	−0.6%	203.0
Penis	1.05	*muscle (newborn/adult)*		28.33		20.32		ND
Scrotum	1.03	*ICRU-46 ave soft tissue*		49.24		34.99		ND
Testes (2)	1.04	*testes (adult)*	33.65	35.06	0.2%	34.93	−0.2%	35.0
Prostate Gland	1.03	*ICRU-46 ave soft tissue*	16.50	17.00	0.0%	16.96	−0.2%	17.0
Skeletal System								
Coastal Cartilage	1.10	*cartilage (adult)*		53.25		49.78		ND
Intervertebral Discs	1.10	*cartilage (adult)*		82.02		65.09		ND
Bone Tissues	1.39	*volume-averaged*	6772.11	9402.06	0.0%	9342.93	−0.6%	9400.0
Bone (CB, TB)	1.90	*cortical bone (ICRP89 Para 436)*						5500.0
Active Marrow [b]	1.03	*red marrow (adult)*						1170.0
Inactive Marrow	0.98	*yellow marrow (adult)*						2480.0
Teeth	3.00	*ICRP 89 - Para 465*						50.0
Miscellaneous [c]	1.03	*ICRU-46 ave soft tissue*						200.0
Integumentary System								
Skin	1.10	*all ages (ICRP89 Para 529)*	3000.00	ND		3687.32	11.7%	3300.0
Additional Tissues								
Adrenal Glands (2)	1.03	*ICRU-46 ave soft tissue*	13.59	13.99	0.0%	13.95	−0.3%	14.0
Brain	1.04	*brain (newborn/infant/adult)*	1394.23	1450.80	0.1%	1449.41	0.0%	1450.0
Breasts (2)	0.94	*adipose#2 (newborn/child/adult)*	26.60	25.02	0.1%	24.89	−0.4%	25.0
Ears	1.10	*cartilage (adult)*		25.87		16.24		ND
External nose	1.05	*66:33 soft tissue/cartilage*		15.31		8.69		ND
Eyes (2)	1.03	*ICRU-46 ave soft tissue*	14.56	15.00	0.0%	14.98	−0.1%	15.0
Lens (2)	1.07	*eye lens (adult)*	0.42	0.45	0.1%	0.45	−0.8%	0.5
Pituitary Gland	1.03	*ICRU-46 ave soft tissue*	0.58	0.60	0.2%	0.60	0.0%	0.6
Spinal Cord	1.04	*brain (newborn/adult)*		124.80		119.94		ND
Spleen	1.06	*spleen (40wk fetus/adult)*	141.51	150.05	0.0%	149.77	−0.2%	150.0
Thymus	1.03	*newborn/adult (ICRP 89 Para 606)*	24.39	24.97	−0.1%	24.85	−0.6%	25.0
Thyroid	1.05	*thyroid (adult)*	19.05	20.05	0.2%	19.97	−0.1%	20.0
Residual Soft Tissues (RST)	1.02					51016.45	−0.8%	51423.6

Organ System	Density (g/cm^3)	Comment (ICRU 46)	Target Volume (cm^3)	UFH - NURBS mass (g)	% Diff	UFH - Voxel mass (g)	% Diff	ICRP 89 mass (g)
Bone-Associated Cartilage [d]	1.10	*cartilage (adult)*						953.0
Separable Fat	0.95	*adipose#2 (newborn/child/adult)*						14500.0
Skeletal Muscle	1.05	*muscle (newborn/adult)*						29000.0
Separable Connective Tissues	1.03	*ICRU-46 ave soft tissue*						2600.0
Fixed Lymphatic Tissues [e]	1.03	*ICRU-46 ave soft tissue*						730.0
Blood (large vessels) [f]	1.06	*blood (newborn/adult)*						1451.5
Miscellaneous RST [g]	1.03	*ICRU-46 ave soft tissue*						2189.0
Totals by Organ System								
Respiratory System (not all tissues have ICRP reference values)				1271.36		1266.23		1238.0
Alimentary System - tissues of organ walls				3328.29		3399.45		3406.0
Alimentary System - GI tract and gall bladder content				958.15		957.69		958.0
Circulatory System - heart wall and content				839.64		838.73		840.0
Urogenital System - kidneys and urinary bladder wall				359.93		359.02		360.0
Urogenital System - urinary bladder content				202.64		201.77		203.0
Urogenital System - internal sex organs (prostate)				17.00		16.96		17.0
Urogenital System - external sex organs (penis, scrotum, and testes)				112.62		90.24		ND
Skeletal System - bone tissues				9402.06		9342.93		9400.0
Integumentary System				ND		3687.32		3300.0
Additional Tissues - excluding residual soft tissue				1866.91		1843.74		1700.1
Additional Tissues - residual soft tissue				ND		51016.45		51423.6
Total Body Tissues						71861	0.25%	71685
Total Body Mass						73021	0.24%	72847

[a] No reference value is given in ICRP 89 and thus an approximate value is used as defined in the ORNL stylized adult phantom

[b] Assumed to include the 7% of total blood volume as per Section 7.7.2 of ICRP 89

[c] As per Section 9.2.15 of ICRP 89, miscellaneous skeletal tissues include periosteum and blood vessels, but exclude periarticular tissue and blood

[d] Skeletal cartilage excludes the following non-bone associated regions of cartilage: external nose and ears, larynx, trachea, and extrapulmonary bronchi

[e] Estimated from the reference adult values given in Section 7.8.2 of ICRP Publication 89 and scaled by total body mass

[f] Taken as 25.92% of total blood pool as per Section 7.7.2 of ICRP 89 (other tissues, arota, large arteries, large veins)

[g] Miscellaneous rest-of-body is added to force the total body mass to its ICRP 89 reference value

Table 3

Summary of organ masses within two computational phantoms of the adult reference female: (1) UF Hybrid-NURBS and (2) UF Hybrid-Voxel. These organ masses are then compared to those in ICRP Publication 89 by organ, organ system, and for total body tissues (exclusive of walled-organ content), and total body mass (inclusive of wall-organ content).

Organ System	Density (g/cm^3)	Comment (ICRU 46)	Target Volume (cm^3)	UFH - NURBS mass (g)	% Diff	UFH - Voxel mass (g)	% Diff	ICRP 89 mass (g)
Respiratory System								
ET1 (anterior nasal layer)	1.02	*ICRU-46 ave soft tissue*		0.36		0.29		ND
ET2 (posterior nasal layer)	1.02	*ICRU-46 ave soft tissue*		1.66		1.47		ND
ET2 (oral cavity layer)	1.02	*ICRU-46 ave soft tissue*		1.15		1.13		ND
ET2 (larynx)	1.07	*50:50 soft tissue/cartilage*	17.84	19.00	0.0%	19.03	0.2%	19.0
ET2 (pharynx)	1.02	*ICRU-46 ave soft tissue*		1.55		1.58		ND
Trachea	1.07	*50:50 soft tissue/cartilage*	7.51	7.99	−0.1%	8.01	0.1%	8.0
Bronchi - extrapulmonary	1.07	*50:50 soft tissue/cartilage*		7.94		7.62		ND
Lungs (inclusive of blood)	0.38	*calculated*	2507.72	950.00	0.0%	947.35	−0.3%	950.0
Left Lung	0.38	*calculated*	1166.38	435.80	−1.4%	433.86	−1.8%	441.9
Right Lung	0.38	*calculated*	1341.34	514.20	1.2%	513.49	1.1%	508.1
Alimentary System								
Tongue	1.05	*muscle*	57.14	60.00	0.0%	59.80	−0.3%	60.0
Salivary glands	1.02	*ICRU-46 ave soft tissue*	68.63	70.06	0.1%	69.68	−0.5%	70.0
Parotid	1.02	*ICRU-46 ave soft tissue*	40.20	41.08	0.2%	40.81	−0.5%	41.0
Submaxillary	1.02	*ICRU-46 ave soft tissue*	20.59	20.97	−0.1%	20.90	−0.5%	21.0
Sublingual	1.02	*ICRU-46 ave soft tissue*	7.84	8.01	0.1%	7.97	−0.4%	8.0
Tonsils	1.02	*ICRU-46 ave soft tissue*	2.94	3.00	−0.1%	2.99	−0.4%	3.0
Esophagus - wall	1.03	*gastrointestine (adult)*	33.98	35.04	0.1%	35.06	0.2%	35.0
Stomach - wall	1.03	*gastrointestine (adult)*	135.92	140.02	0.0%	139.65	−0.3%	140.0
Stomach - contents	1.02	*ICRU-46 ave soft tissue*	225.49	230.15	0.1%	231.14	0.5%	230.0
Small Intestine - wall	1.03	*gastrointestine (adult)*	582.52	603.41	0.6%	595.71	−0.7%	600.0
Small Intestine - contents	0.56	*ICRU-46 ave soft tissue*	502.07	280.00	0.0%	279.00	−0.4%	280.0
Colon								
Right - wall	1.03	*gastrointestine (adult)*	140.78	145.00	0.0%	144.42	−0.4%	145.0
Right - contents	1.74	*ICRU-46 ave soft tissue*	92.19	160.00	0.0%	159.62	−0.2%	160.0
Left - wall	1.03	*gastrointestine (adult)*	140.78	144.92	−0.1%	144.50	−0.3%	145.0
Left - contents	0.55	*ICRU-46 ave soft tissue*	144.56	80.00	0.0%	79.69	−0.4%	80.0
Rectosigmoid - wall	1.03	*gastrointestine (adult)*	67.96	70.54	0.8%	69.94	−0.1%	70.0
Rectosigmoid - contents	0.82	*ICRU-46 ave soft tissue*	97.14	80.00	0.0%	79.86	−0.2%	80.0
Liver	1.06	*liver (fetus/child/adult)*	1320.75	1400.55	0.0%	1397.57	−0.2%	1400.0
Gall Bladder - wall	1.02	*ICRU-46 ave soft tissue*	7.84	7.99	−0.1%	7.95	−0.6%	8.0
Gall Bladder - contents	1.02	*ICRU-46 ave soft tissue*	47.06	48.02	0.0%	47.91	−0.2%	48.0
Pancreas	1.02	*ICRU-46 ave soft tissue*	117.65	120.00	0.0%	119.89	−0.1%	120.0
Circulatory System								

Organ System	Density (g/cm^3)	Comment (ICRU 46)	Target Volume (cm^3)	UFH - NURBS mass (g)	% Diff	UFH - Voxel mass (g)	% Diff	ICRP 89 mass (g)
Heart - wall	1.05	*heart (fetus/child/adult)*	238.10	250.42	0.2%	249.98	0.0%	250.0
Heart - content	1.06	*blood (newborn/adult)*	349.06	369.95	0.0%	369.17	−0.2%	370.0
Urogenital System								
Kidneys (Cortex+Medulla)	1.05	*kidney (fetus/child/adult)*	261.90	274.82	−0.1%	274.17	−0.3%	275.0
Cortex (70%)	1.05	*kidney (fetus/child/adult)*	192.98	202.51	−0.1%	201.89	−0.4%	202.6
Medulla (25%)	1.05	*kidney (fetus/child/adult)*	68.92	72.31	−0.1%	72.28	−0.1%	72.4
Pelvis (5%)	1.05	*kidney (fetus/child/adult)*	13.78	14.46	−0.1%	14.46	−0.1%	14.5
Urinary Bladder - wall	1.04	*bladder (adult-empty)*	38.46	40.15	0.4%	39.94	−0.1%	40.0
Urinary Bladder - contents[a]	1.01	*urine of ave density*	160.79	162.54	0.1%	161.76	−0.4%	162.4
Ovaries (2)	1.05	*ovaries (adult)*	10.48	11.00	0.0%	10.96	−0.4%	11.0
Uterus	1.05	*muscle (newborn/adult)*	76.19	79.95	−0.1%	79.83	−0.2%	80.0
Skeletal System								
Coastal Cartilage	1.10	*cartilage (adult)*		41.39		37.96		ND
Intervertebral Discs	1.10	*cartilage (adult)*		68.41		56.53		ND
Bone Tissues	1.38	*volume-averaged*	4985.98	6903.98	0.1%	6879.15	−0.3%	6900.0
Bone (CB, TB)	1.90	*cortical bone (ICRP89 Para 436)*						4000.0
Active Marrow [b]	1.03	*red marrow (adult)*						900.0
Inactive Marrow	0.98	*yellow marrow (adult)*						1800.0
Teeth	3.00	*ICRP 89 - Para 465*						40.0
Miscellaneous [c]	1.02	*ICRU-46 ave soft tissue*						160.0
Integumentary System								
Skin	1.10	*all ages (ICRP89 Para 529)*	2090.91	ND		2571.80	11.8%	2300.0
Additional Tissues								
Adrenal Glands (2)	1.02	*ICRU-46 ave soft tissue*	12.75	13.02	0.1%	12.96	−0.3%	13.0
Brain	1.04	*brain (newborn/infant/adult)*	1250.00	1300.47	0.0%	1298.13	−0.1%	1300.0
Breasts (2)	0.94	*adipose#2 (newborn/child/adult)*	531.91	500.21	0.0%	499.79	0.0%	500.0
Ears	1.10	*cartilage (adult)*		9.47		6.96		ND
External nose	1.05	*66:33 soft tissue/cartilage*		4.67		5.01		ND
Eyes (2)	1.02	*ICRU-46 ave soft tissue*	14.71	14.98	−0.1%	14.92	−0.6%	15.0
Lens (2)	1.07	*eye lens (adult)*	0.42	0.45	−0.1%	0.45	0.8%	0.5
Pituitary Gland	1.02	*ICRU-46 ave soft tissue*	0.59	0.60	0.2%	0.60	0.7%	0.6
Spinal Cord	1.04	*brain (newborn/adult)*		48.76		47.82		ND
Spleen	1.06	*spleen (40wk fetus/adult)*	122.64	130.15	0.1%	129.80	−0.2%	130.0
Thymus	1.03	*newborn/adult (ICRP 89 Para 606)*	19.51	20.01	0.0%	19.91	−0.5%	20.0
Thyroid	1.05	*thyroid (adult)*	16.19	17.00	0.0%	16.97	−0.2%	17.0
Residual Soft Tissues (RST)	1.00					42601.14	−0.7%	42880.4
Bone-Associated Cartilage [d]	1.10	*cartilage (adult)*						894.7

Organ System	Density (g/cm^3)	Comment (ICRU 46)	Target Volume (cm^3)	UFH - NURBS mass (g)	% Diff	UFH - Voxel mass (g)	% Diff	ICRP 89 mass (g)
Separable Fat	0.95	*adipose#2 (newborn/child/adult)*						19000.0
Skeletal Muscle	1.05	*muscle (newborn/adult)*						17500.0
Separable Connective Tissues	1.02	*ICRU-46 ave soft tissue*						2100.0
Fixed Lymphatic Tissues [e]	1.02	*ICRU-46 ave soft tissue*						600.0
Blood (large vessels) [f]	1.06	*blood (newborn/adult)*						1062.7
Miscellaneous RST [g]	1.02	*ICRU-46 ave soft tissue*						1723.0
Totals by Organ System								
Respiratory System (not all tissues have ICRP reference values)				989.64		986.48		977.0
Alimentary System - tissues of organ walls				2870.59		2856.85		2866.0
Alimentary System - GI tract and gall bladder content				878.17		877.23		878.0
Circulatory System - heart wall and content				620.38		619.15		620.0
Urogenital System - kidneys, urinary bladder wall, ureters				314.97		314.11		315.0
Urogenital System - urinary bladder content				162.54		161.76		162.4
Urogenital System - internal sex organs (ovaries and uterus)				90.96		90.79		91.0
Skeletal System - bone tissues				6903.98		6879.15		6900.0
Integumentary System				ND		2571.80		2300.0
Additional Tissues - excluding residual soft tissue				2059.77		2053.31		1996.1
Additional Tissues - residual soft tissue				ND		42601.14		42880.4
Total Body Tissues						58973	0.05%	58945
Total Body Mass						60012	0.04%	59986

[a] No reference value is given in ICRP 89 and thus an approximate value is used as defined in the ORNL stylized adult phantom

[b] Assumed to include the 7% of total blood volume as per Section 7.7.2 of ICRP 89

[c] As per Section 9.2.15 of ICRP 89, miscellaneous skeletal tissues include periosteum and blood vessels, but exclude periarticular tissue and blood

[d] Skeletal cartilage excludes the following non-bone associated regions of cartilage: external nose and ears, larynx, trachea, and extrapulmonary bronchi

[e] Estimated from the reference adult values given in Section 7.8.2 of ICRP Publication 89 and scaled by total body mass

[f] Taken as 25.92% of total blood pool as per Section 7.7.2 of ICRP 89 (other tissues, arota, large arteries, large veins)

[g] Miscellaneous rest-of-body is added to force the total body mass to its ICRP 89 reference value